Computational modelling of a triaxial vibrating sample magnetometer

Cite as: AIP Advances 14, 025306 (2024); doi: 10.1063/9.0000787
Submitted: 3 October 2023 • Accepted: 25 November 2023 •
Published Online: 2 February 2024

Leo Rodriguez,[1,a)] Arjun Sapkota,[2] Jonathan Alvarado,[3] Jitendra S. Tate,[1] and Wilhelmus J. Geerts[1]

AFFILIATIONS

[1] Materials Science, Engineering and Commercialization, Texas State University, San Marcos, Texas 78666, USA
[2] Department of Physics, Texas State University, San Marcos, Texas 78666, USA
[3] Mechanical Engineering, University of Texas Rio Grande Valley, Edinburg, Texas 78539, USA

Note: This paper was presented at the 68th Annual Conference on Magnetism and Magnetic Materials.
[a)]**Author to whom correspondence should be addressed:** l_r217@txstate.edu

ABSTRACT

Magnetic Field Assisted Additive Manufacturing (MFAAM) enables 3D printing of magnetic materials of various shapes which exhibit a complex anisotropy energy surface containing contributions generated from different origins such as sample, particle, and agglomerate shape anisotropy, flow and field induced anisotropy, and particle crystal anisotropy. These novel magnet shapes require the need to measure the x, y, and z components of the magnetic dipole moment simultaneously to fully understand the magnetic reversal mechanism and unravel the complex magnetic anisotropy energy surface of 3D printed magnetic composites. This work aims to develop a triaxial vibrating sample magnetometer (VSM) by adding a z-coil set to a pre-existing biaxial VSM employing a modified Mallison coil set. The optimum size and location of the sensing coils were determined by modeling the sensitivity matrix of the z-coil set. The designed coil set was implemented using 3D printed spools, a manual coil winder, and gauge 38 copper wire. A 3D printed strontium ferrite nylon composite sample was used to estimate the sensitivity of the z-coils (50 mV/emu). The results herein are applicable for any VSM using a modified Mallison biaxial coil configuration allowing for a quick implementation on pre-existing systems.

I. INTRODUCTION

A Vibrating Sample Magnetometer (VSM) measures the magnetic moment of materials as a function of an applied field, the field angle, and the temperature.[1] These data help determine magnetic properties such as Magnetic moment per unit volume, magnetic anisotropy (MA), and exchange coupling. Sensing pickup coils are placed around a vibrating sample exposed to a magnetic field. The sample's magnetic dipole moment creates a time varying field that (through Faraday's law of induction) is sensed by the pickup coils.[2] In VSMs that use a resistive electromagnet, the sample is vibrated perpendicular to the magnetic field. VSM development started in the 1950s by Foner[1] and Foner[3] independently. Foner published several papers which helped improve the design of the detection system and consequently VSMs are also called a Foner magnetometer.[3–5]

MA describes how magnetic properties vary depending on the applied magnetic field direction. MA is important for applications including permanent magnets, magnetic recording media and read heads.[6] Anisotropic ferromagnetic materials exhibit an easy (magnetic moment preferential direction) and hard axis for magnetization.[7] MA can be measured directly (torque measurement as a function of the applied field and angle) or indirectly (field angle dependence of a hysteresis curve). Torque is not observed in a saturated anisotropic material when the easy axis is aligned with the magnetic field but is present for other field angles. This field angle dependence of the torque is a measure of MA and can be used to calculate information on the MA energy surface of the material.[8] A hysteresis (M-H) curve is the relation between magnetization (M) and the field strength (H) and is referred to as the material's magnetic fingerprint.[9] The M-H curve's shape depends on extrinsic properties such as defects, texture, and crystal size, and morphology and also on intrinsic properties such as magnetization, exchange interaction and MA constant. If H is orientated in the x direction and **M** has non-zero components perpendicular to x, a torque **T** is exerted on the sample given by:[10]

$$\vec{T} = M_z H_x \hat{y} + M_y H_x \hat{z} \quad (1)$$

Complex MA energy surfaces can arise from sample shape, flow, and an applied magnetic field during deposition.[11] Currently, most torque magnetometers only measure the scalar torque curve.[12] To measure materials with a complex MA energy surface (multiple competing anisotropies) a vector torque magnetometer is required. A triaxial VSM (TVSM) would be capable of measuring all three components of the magnetic moment. A few research groups have previously built their own TVSMs, however, most are no longer in use or have been dismantled (thin film sample symmetry is often sufficient to determine the MA with a scalar instrument).[13–16] While biaxial VSMs are commercially available there are presently no commercial TVSMs, so this work aims to fill that gap by developing a TVSM by modifying a preexisting biaxial VSM (BVSM).[17]

II. COIL DESIGN

Pickup coil design has been discussed by Bernards, Richter *et al.*, Samwel *et al.*, and Tumanski.[18–20] The BVSM has a modified Mallison coil system consisting of 2 pairs of coils to measure the x and y components of the sample's magnetic dipole moment. The x and y-coils axes are aligned parallel and perpendicular to the applied magnetic field, respectively. These two coil pairs are enclosed in a grounded aluminum coil-box attached to the pole pieces of the resistive electromagnet. Two different z-coil configurations (Fig. SI-1) were explored. For the 4-coil configuration, two coil pairs with their cylindrical axis parallel to the sample rod are placed in front and behind the coil-box. This approach is similar to Benito *et al.*[16] We also explored a 2-coil configuration with coils centred around the sample rod, above and below the sample. This method was implemented in a TVSM by Matsubara *et al.*[13] and is often used in VSMs using a superconducting magnet.[21] The 4-coil configuration allows usage of coils with a small-bore diameter positioned farther away from the sample. The 2-coil configuration limits bore diameter but allowed the coils to be positioned close to the sample using an outer diameter that fits inside the biaxial coil-box. Good coil design will maximize the sensitivity for the M_z component (S_{zz}) but will minimize cross-talk of the M_y and M_x into the Z-coils (S_{zx}, S_{zy})[22] while allowing a certain sample size. Also, the dependence of sensitivity and cross-talk on sample position, and materials/equipment cost should be minimized.

The TVSM design focused on the z-coil sensitivity and cross-talk using the reciprocity theorem and the magnetic scalar potential. Bernards mathematical framework was used to model the coil sensitivity and cross-talk.[23] The scalar magnetic potential for an azimuthal symmetric current distribution (such as the pick-up coils) can be written by a Legendre polynomial series. For a coil centred around the z-axis and positioned at the origin, the scalar potential for large r is given by

$$V_c(\theta, r) = \sum_{l=1,3,5} B_l \frac{1}{r^{l+1}} P_l(\theta) \tag{2}$$

Where P_l are the Legendre polynomials, θ,r are the cylindrical coordinates of the field point away from the coil, and B_l are constants that depend on the shape and size of the coil determined for a coil with finite dimensions by Zijlstra.[24] For a sample vibrating in the z-direction the S_{zz}, S_{zx}, and S_{zy} can be derived from the reciprocity theorem:[25]

$$S_{zi} = \frac{\partial^2}{\partial z \partial i} V_c(z, r) \tag{3}$$

Where i is x, y, or z and the sensitivities are unitless values. Mathematica[26] was used to model and optimize the coil configurations, dimensions and positions. A target coil sensitivity was first computed based on a real-world BVSM system. For the 4-coil configuration sensitivity was then computed by optimizing the coil position, coil inner bore (C_b), coil length (C_l) and coil outer diameter (C_d) toward the target sensitivity. The 2-coil system was optimized slightly differently due to the need to support the coils inside the box. The 2-coils were placed outside the coil-box where the C_d was optimized and then moved toward the sample (inside the coil-box along the z-axis). Finally, C_l was optimized toward the target sensitivity.

III. RESULTS AND DISCUSSION

The estimated sensitivity for the x-coil set in our VSM is ~0.046 and was used as a target value for the z-coil set design.

For the 4-coil configuration the position of the coils along the z-direction is first modelled for three different C_b values. The calculations show that as C_b shrinks the estimated sensitivity increases. An optimum distance between the coils in the z-position seems to exist for which S_{zz} is maximum (Fig. SI-2). Machinery limitations used for coil winding forced the use of a C_b of 5.3 mm with an optimal z position of the coils 8 mm above and below the sample resulting in a maximum sensitivity value of 0.0027. Further C_l optimization brings the maximum sensitivity value to 0.0033 (using C_l = 14 mm). 14 mm was the maximum allowable C_l as larger values would intrude on the sample mounting area thereby reducing the maximum sample size. Finally, C_d increased the S_{zz} for a centred sample to 0.013 05 (Fig. SI-2) which falls 112% short of the 0.046 target sensitivity. Thus the 4-coil setup was determined to be a nonviable option for use with the pre-existing VSM as it would result in a z-sensitivity that is significantly lower than the x and y-sensitivities.

The 2-coil configuration is constrained by the dimensions of the coil-box of our BVSM. Placing z-coils above and below the coil-box (z = ±26 on the z-axis) allows one to use large coil diameters, but negatively impacts sensitivity since the coils are farther away from the sample. Coils with a C_d of 32 mm positioned at z = ±26 mm gives a S_z of 0.012. This is a 115% reduction compared to a coil with a C_d of 16 mm that fits in the coil-box positioned at z = ±11. This shows that a coil positioned closer to the sample increases coil-sample coupling and provides greater S_z as opposed to larger coils placed farther away as was also mentioned by Dodrill.[27] The maximum sample size will further constrain the minimum bore diameter as the coils are straddled around the sample rod. To allow samples up to 8 mm diameter to be measured the C_b was increased from 5.3 mm to 10.8 mm. To compensate for the reduction of S_{zz} the length of the coil was increased from 2 to 3 mm (Fig. SI-5) to obtain the set target sensitivity for the z-coil set (0.046).

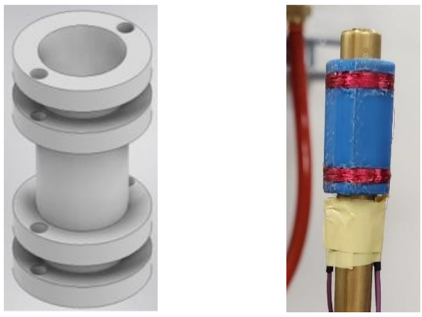

FIG. 1. Initial CAD rendering of 2-coil spool (left) and finished 3D printed spool and z-coils (right).

IV. IMPLEMENTATION AND VERIFICATION

A fused deposition modeling 3D printer (Flsun QQ-S) with Polylactic Acid (PLA) filament was used to construct a spool for the optimized z-coil set (Fig. 1). The coils were wound using a manual NZ-2 coil winding machine using AWG38 copper wires with a diameter of 0.099 06 mm (with a calculated cross-sectional area of 0.007 707 mm^2) coated with a thin layer of insulated enamel and mounted on a thin wall brass tube (thickness of 0.2 mm). This tube was inserted in a post-holder and mounted on a mechanical stage which allowed for three translation (x, y, z) and three rotation axes (q_x, q_y, q_z) adjustments. The stage was secured to a slide mount under the electromagnet. Assuming square packing of the coil wires, the ideal wire length can be estimated using the coil dimensions and wire diameter given by Eq. (4):

$$W_{length} = \int_{C_b/2}^{C_d/2} \frac{2\pi r C_l}{W_{diameter}^2} dr \tag{4}$$

The ideal calculated wire length for the coils is 33.5 m. An approximate wire length L of each coil was calculated using the measured resistance R:

$$R = \rho \frac{L}{A} \tag{5}$$

where ρ is the resistivity of annealed copper (1.7×10^{-5} Ω mm),[28] and A is the cross-sectional area of the wire ($A = \pi r^2$, r = wire radius). Multimeter coil resistance measurements were 57 and 52 Ohm for the top and bottom coils with an estimated coil length of 25.8 and 23.6 m, respectively. The lower measured length demonstrates the coil packing is not square and neither perfect. Careful inspection during the coil winding process indicates coil wire packing is impacted by the spool (Fig. 1) surface quality.

A 54wt% strontium ferrite/nylon composite wire shaped sample (mass = 2.05 mg, 4 x 0.2 x 0.7 mm) made using magnetic field assisted additive manufacturing (MFAAM) was used to calibrate and test the z-coil set. The sample was 3D-printed in a magnetic field resulting in a distinct but canted easy axis in a plane defined by the print bed normal and the print direction (Fig. SI-6).[29]

M-H curves of the sample along the print bed normal were measured with the x and y-coil sets with the sample mounted horizontally on a perpendicular sample rod. M-H curves of the sample with the x and z-coil sets were done with the sample was mounted vertically in a glass rod with an inner diameter of 1 mm (Fig. SI-8). Prior to each measurement the sample was centred with respect to the x-coil set in a magnetic field of 22 000 Oe by adjusting the sample's y and z-positions to maximize the x-coil signal and adjusting the sample's x-position to minimize the x-coil signal. This process was repeated at least three times to guarantee a well-centred sample. M-H curves for both sample mounting configurations were captured using a field range of ±22 000 Oe in sweep mode at 400 Oe/s. As both measurement configurations are identical, the measurements obtained with the y-coil set on the horizontally mounted sample should be identical to measurements obtained with the z-coil set on the vertically mounted sample. Comparing the M_y hysteresis curve of the horizontally mounted sample with the M_z hysteresis curve of the vertically mounted sample, we can determine the calibration factor for the z-coil set.

Prior to the xz measurements the z-coil set was raised in the post holder until approximately centred around the sample and locked in place. The z-coils used thick wires, so a transformer preamplifier (SRS554) was added to boost the z-coil signal and avoid impact of the lockin-amplifier noise. Both z-coils were connected in series to the preamplifier which was connected to the lockin-amplifier of the BVSM. Using the translation stage, fine adjustments to the z-coil's z-position were made by minimizing the z-coil signal while the sample was saturated along the field direction (x) by an applied field of 22 000 Oe.

M-H curves taken of the sample mounted vertically and horizontally are shown in Fig. 2. The remanence values of both hysteresis curves are used to calculate the total sensitivity of the z-coils. The remanence of M_y is 0.0204 emu and the remanence of M_z is 1.0289 mV. Dividing M_z by M_y gives a sensitivity of 50 mV/emu for the TVSM z-coils. This is roughly 10 times higher than the y-coils (5.8 mv/emu). Note that no preamplifier is used for the y-coils. The preamplifier adds an additional term to the total voltage for a N coil configuration given by Bernard[23] as

$$V_{tot} = A_2 \mu_0 M_x V v \frac{N}{A_1} \sum_{i=1}^{n} \pm S_x \tag{6}$$

where N is the number of windings, A_1 is the surface area of a cross section of the coil, and A_2 is the voltage amplification of the preamplifier. In addition, the BVSM x and y-coil sets use a smaller diameter wire allowing a larger number of windings (without using a preamplifier) compared to our z-coils. The amplitude response for the

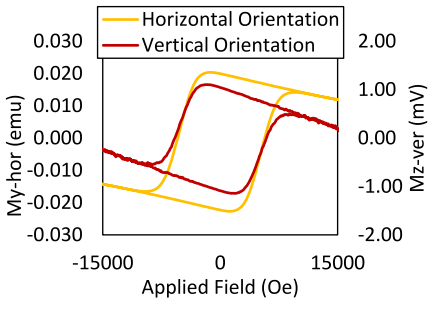

FIG. 2. M-H of vertically and horizontally orientated $SrFe_{12}O_{19}$ sample.

SRS554 at 75 Hz is roughly 37.5 dB.[30] Using Eq. (7) the amplitude was calculated to be 75.

$$A = 10^{\frac{dB}{20}} \tag{7}$$

Dividing the square of the TVSM wire diameter by the square of the BVSM wire diameter gives a cross-sectional area difference factor of 8. Dividing the derived amplitude by the cross-sectional factor gives a value of 9.5. Meaning the TVSM coils are roughly 10 times more sensitive than the y-coils of the BVSM confirming the earlier calculated sensitivity factor (S_x) for the z-coils from the M-H curves. The signal of all three coil sets are shown in Figure SI-7. At large fields the sample reaches saturation in the x-direction and the magnetic moments rotates away from the easy axis and is completely aligned with the magnetic field. At low field the magnetic moment rotates away from the field direction (x-direction) as confirmed by the non-zero M_y and M_z components. The M_y and M_z components at low field are 9% and 25% of M_s respectively. Additionally, a large background noise in the M_z data is attributed to coil vibration from the magnetic field due to contact with the coil-box as they are too large. The noise increases as the field increases suggesting coil vibrations rather than power supply noise is the underlying issue for the observed noise. The z-coils are also not enclosed in any casing making them susceptible to outside interference. The large background slope on the M_z coil also suggest that cross-talk is present on the z-coil signal.

V. CONCLUSIONS

A triaxial VSM z-coil set was modelled and constructed. Computational modeling has shown that an optimal coil configuration (highest S_{zz} and lowest amount of copper) should utilize 2 coils encircling the sample rod above and below the sample. Larger coils placed outside the coil-box lower z-coil sensitivity. The designed z-coil set was implemented using 3D printed spools and thin-wall brass tubing using 38 Gauge copper wire. The measured resistance of the z-coil set indicates that the coils are not optimally wound. A $SrFe_{12}O_{19}$/PA12 3D printed MFAAM sample was used to calibrate the z-coil set. The z-coils sensitivity was estimated to be 50 mV/emu when using a transformer preamplifier. A background noise was detected in the z-coils and increased as the field strength increased likely due to coil vibration. Future coil winding, sample alignment, and coil size improvements are in progress to improve the z-coils to eliminate cross-talk and background noise, and provide greater measurement accuracy. While biaxial VSMs are commercially available, there are presently no commercial triaxial VSMs and this modified VSM can be used to make accurate true vector measurements for materials with a complex anisotropic energy surface such as MFAAM samples.[31]

SUPPLEMENTARY MATERIAL

The supplementary information includes: a diagram of the z-coils configurations tested, optimization trending graphs for the sensitivity matrix of the z-coils, a diagram of the the printing setup for the strontium ferrite sample, a M-H curve for the strontium ferrite sample showing all three components, and a diagram of the strontium ferrite sample in a vertical and horizontal orientation.

ACKNOWLEDGMENTS

This work was supported in part by NSF through DMR-MRI Grant under awards 2216440 and in part by DOD instrumentation grant (78810-W911NF-21-1-0253). L.R. would like to thank Dr. Erik Samwel of MicroSense KLA for constructive feedback.

AUTHOR DECLARATIONS

Conflict of Interest

The authors have no conflicts to disclose.

Author Contributions

Leo Rodriguez: Conceptualization (equal); Data curation (equal); Formal analysis (equal); Investigation (equal); Methodology (equal); Validation (equal); Visualization (equal); Writing – original draft (equal); Writing – review & editing (equal). **Arjun Sapkota**: Investigation (equal); Methodology (equal). **Jonathan Alvarado**: Investigation (equal); Methodology (equal). **Jitendra S. Tate**: Funding acquisition (equal); Resources (equal); Supervision (equal). **Wilhelmus J. Geerts**: Funding acquisition (equal); Project administration (equal); Resources (equal); Supervision (equal); Validation (equal).

DATA AVAILABILITY

The data that support the findings of this study are available from the corresponding author upon reasonable request.

REFERENCES

[1] S. Foner, "Versatile and sensitive vibrating-sample magnetometer," Rev. Sci. Instrum. **30**(7), 548–557 (1959).
[2] B. Dodrill and J. R. Lindemuth, "Vibrating sample magnetometry," in *Magnetic Measurement Techniques for Materials Characterization*, edited by V. Franco and B. Dodrill (Springer International Publishing, 2021), pp. 15–37.
[3] S. Foner, "Further improvements in vibrating sample magnetometer sensitivity," Rev. Sci. Instrum. **46**(10), 1425–1426 (1975).
[4] S. Foner, "Review of magnetometry," IEEE Trans. Magn. **17**(6), 3358–3363 (1981).
[5] S. Foner, "The vibrating sample magnetometer: Experiences of a volunteer (invited)," J. Appl. Phys. **79**(8), 4740–4745 (1996).
[6] B. C. Dodrill, "Measurements with a VSM: Magnetic media," Lakeshore Cryotronics, Application Note, 2001.
[7] M. T. Johnson, P. J. H. Bloemen, F. J. A. den Broeder, and J. J. de Vries, "Magnetic anisotropy in metallic multilayers," Reports Prog. Phys. **59**(11), 1409 (1996).
[8] D. Jiles, *Introduction to Magnetism and Magnetic Materials*, 3rd ed. (CRC Press, Boca Raton, 2015).
[9] C. D. G. B. D. Cullity, *Introduction to Magnetic Materials*, 2nd ed. (Wiley, 2009).
[10] S. Chikazumi, *Physics of Ferromagnetism*, 2nd ed. (Clarendon Press, Oxford, 1997).

[11] L. Henderson *et al.*, "Altering magnetic properties of iron filament PLA using magnetic field assisted additive manufacturing (MFAAM)," J. Magn. Magn. Mater. **538**, 168320 (2021).
[12] K. R. Fast *et al.*, "Simultaneous three-axis torque measurements of micromagnetism," AIP Adv. **11**(1), 15119 (2021).
[13] N. Matsubara and F. Sai, "Measurement of magnetization of an obliquely deposited film by using 3-dimensional vector VSM," IEEE Trans. Magn. **27**(6), 4748–4750 (1991).
[14] A. N. Bazhan, "Three coordinate vibrating sample magnetometer," J. Magn. Magn. Mater. **157–158**, 569–570 (1996).
[15] M. Le Goff and Y. Gallet, "A new three-axis vibrating sample magnetometer for continuous high-temperature magnetization measurements: Applications to paleo- and archeo-intensity determinations," Earth Planet. Sci. Lett. **229**, 31 (2004).
[16] L. Benito, J. I. Arnaudas, and A. del Moral, "High-sensitivity vector magnetometer for measuring magnetic torque at low temperatures," Rev. Sci. Instrum. **77**(2), 25101 (2006).
[17] "MicroSense EZ9-HF." Lowell, [Online]. Available: http://www.microsense.net/index.htm
[18] H. J. Richter, "On the construction of detection coils for a vectorial vibrating sample magnetometer," J. Magn. Magn. Mater. **111**(1–2), 201–213 (1992).
[19] E. O. Samwel, T. Bolhuis, and J. C. Lodder, "An alternative approach to vector vibrating sample magnetometer detection coil setup," Rev. Sci. Instrum. **69**(9), 3204–3209 (1998).
[20] S. Tumanski, "Induction coil sensors—A review," Meas. Sci. Technol. **18**(3), R31 (2007).
[21] M. Springford, J. R. Stockton, and W. R. Wampler, "A vibrating sample magnetometer for use with a superconducting magnet," J. Phys. E. **4**(12), 1036 (1971).
[22] T. Bolhuis, L. Abelmann, J. C. Lodder, and E. O. Samwel, "On the vectorial calibration of a vibrating sample magnetometer for thin film measurements," J. Magn. Magn. Mater. **193**(1–3), 332–336 (1999).
[23] J. P. C. Bernards, "Design of a detection coil system for a biaxial vibrating sample magnetometer and some applications," Rev. Sci. Instrum. **64**(7), 1918–1930 (1993).
[24] H. Zijlstra, *Experimental Methods in Magnetism* (North-Holland Publishing Company, 1967), Vol. 1.
[25] J. Mallinson, "Magnetometer coils and reciprocity," J. Appl. Phys. **37**(6), 2514–2515 (1966).
[26] I. Wolfram Research, Mathematica (Wolfram Research, Inc., Champaign, Illinois, 2023) [Online]. Available: https://www.wolfram.com/mathematica.
[27] B. C. Dodrill, "Magnetometry measurements of nanomagnetic materials," Adv. Mater. TechConnect Briefs (2018).
[28] R. C. Weast, *CRC Handbook of Chemistry and Physics* (CRC Press, 1981).
[29] T. N. Ahmed, "Magnetic and morphological characterization of $SrFe_{12}O_{19}/PA_{12}$ composites: Hard-magnetic filament for magnetic field assisted additive manufacturing (MFAAM)" (Texas State University, 2023).
[30] S. R. Systems, "SR554 transformer preamplifier specifications," https://www.thinksrs.com/products/sr554.html; accessed 01 Nov. 2023.
[31] T. N. Ahmed, C. Selsor, J. S. Tate, and W. J. Geerts, "Magnetic behavior and chaining of strontium ferrite-nylon composite above the melting temperature," AIP Adv. **13**(2), 25024 (2023).